

Band geometry from position-momentum duality at topological band crossings

Yu-Ping Lin¹ and Wei-Han Hsiao²

¹*Department of Physics, University of Colorado, Boulder, Colorado 80309, USA*

²*Independent Researcher*

(Dated: February 28, 2025)

We show that the position-momentum duality offers a transparent interpretation of the band geometry at the topological band crossings. Under the position-momentum duality, the band geometry with Berry connection is dual to the free-electron motion under gauge field. This identifies the trace of quantum metric as the dual energy in momentum space. The band crossings with Berry defects can induce the dual energy quantization in the trace of quantum metric. For a \mathbb{Z} nodal-point or nodal-surface semimetal, a dual Landau level quantization occurs owing to the Berry charge. Meanwhile, a nodal-loop semimetal exhibits a Berry vortex line, leading to the dual rotational energy about the nodal loop. A \mathbb{Z}_2 monopole further brings about another dual rotational energy, which originates from the link with an additional nodal line. Nontrivial band geometry generically induces finite spread in the Wannier functions. While the spread manifests a quantized lower bound in a \mathbb{Z} nodal-point or nodal-surface semimetal, logarithmic divergence occurs in a nodal-loop semimetal. The band geometry at the band crossings may be probed experimentally by a periodic-drive measurement.

The modern study of gapless topological systems have uncovered various unconventional band structures with fascinating phenomena. These systems accommodate band crossings in the Brillouin zone, where nontrivial band topology may occur. A band crossing in the three-dimensional (3D) Brillouin zone may occur at a nodal point, a nodal line, or a nodal surface (Fig. 1) [1, 2]. These band crossings are realized in the semimetallic phases of solid-state materials, including the nodal-point [2–12], nodal-line [2, 13–19], and nodal-surface [16, 18, 20, 21] semimetals. The topological superconductors [22–27] and the spin liquids [28] can also host the band crossings in the low-energy quasiparticle spectrum. Furthermore, recent studies of synthetic topological systems present another set of platforms for the bands crossings to occur. These include the ultracold atomic systems [29, 30], the photonic systems [31], and the superconducting circuits [32, 33].

The band topology may exhibit different forms from different band crossings, which are classified based on the symmetries and the band-crossing structures [1]. For the 3D gapless topological systems, the topological classifications involve the \mathbb{Z} and \mathbb{Z}_2 classifications. Various types of integer topological invariants are proposed as the indicators of these topological classifications. For example, a nodal point with \mathbb{Z} classification [Fig. 1(a)] carries a Berry monopole, leading to a quantized Chern number under an enclosing-surface integration [34]. A \mathbb{Z} nodal point may be inflated into a \mathbb{Z} nodal surface [Fig. 1(b)] [24, 25], where the framework of Berry charge still apply [20]. On the other hand, a nodal line in a combined parity and time-reversal PT symmetric system can carry a \mathbb{Z}_2 monopole [15, 17]. The according topological invariant corresponds to the linking number with additional nodal lines [Fig. 1(d)] [19].

The band crossings also lead to nontrivial quantum ge-

ometry of the bands [35]. The band geometry is characterized by the quantum metric, which measures the state variation under momentum change [36–38]. The components of quantum metric may be probed experimentally, for example, by a periodic drive [39]. Recent studies have uncovered various manifestations of the quantum metric. The integrated trace of quantum metric defines a lower bound of the spread of Wannier functions [40–42]. Such a lower bound can be measured directly in the experimental systems [39, 43–48]. The spread of Wannier functions can trigger anomalous superfluid stiffness on flat bands, leading to the geometric enhancement of flat-band superconductivity [49–53]. It can also lead to finite current noise even in the insulating phase [54]. Other works have adopted the quantum metric as an indicator of phase transitions [55–57], fractional Chern insulators [58, 59], excitons [60], and orbital susceptibilities [61, 62].

Most of the previous works have focused on the extrinsic manifestations of the quantum metric. Meanwhile, the intrinsic character of the quantum metric has not received sufficient investigation. The studies along this direction have been conducted recently in the context of nodal-point semimetals. The trace of quantum metric receives a transparent interpretation in the chiral multifold semimetals [35]. Under the position-momentum duality to the Haldane sphere [63], the trace of quantum metric is identified as the dual energy in momentum space, thereby acquiring a dual Landau level quantization from the Berry monopole. On the other hand, the integrated determinant of quantum metric over an enclosing surface is proposed as a measure of the Berry defect [64, 65]. These results exemplify the nature of the quantum metric at the nodal points. A natural question then arises as whether these scenarios can be generalized to the band geometry in the other topological systems.

In this Letter, we show that the position-momentum

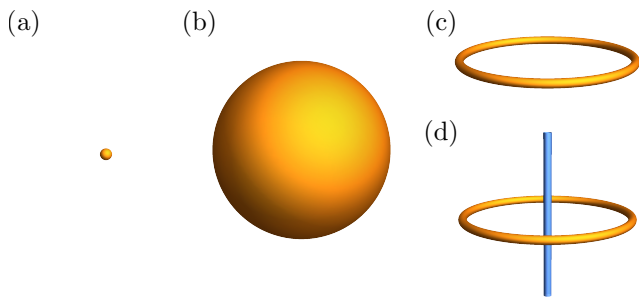


FIG. 1. Band crossings in the 3D Brillouin zone. (a) Nodal point. (b) Nodal surface. (c) \mathbb{Z}_2 -trivial nodal loop. (d) \mathbb{Z}_2 -nontrivial nodal loop.

duality [35] offers a unified framework of the band geometry at the topological band crossings. Under the position-momentum duality, the band geometry with Berry connection is dual to the free-electron motion under gauge field. This identifies the trace of quantum metric as the dual energy in momentum space. The band crossings with Berry defects can induce the dual energy quantization in the trace of quantum metric. For a \mathbb{Z} nodal-point or nodal-surface semimetal, a dual Landau level quantization occurs owing to the Berry charge. Meanwhile, a nodal-loop semimetal exhibits a Berry vortex line, leading to the dual rotational energy about the nodal loop. A \mathbb{Z}_2 monopole further brings about another dual rotational energy, which originates from the link with an additional nodal line. The spread of Wannier functions manifests a quantized lower bound in a \mathbb{Z} nodal-point or nodal-surface semimetal, while logarithmic divergence occurs in a nodal-loop semimetal. Our duality-based analysis paves the way for advanced comprehension of nontrivial band geometry at the topological band crossings.

We begin with an introduction to the band geometry. Consider a band with the Bloch eigenstate $|u_{\mathbf{k}}\rangle$, which generically evolves under the variation of momentum \mathbf{k} . Such an evolution manifests the variations in the phase and the state. A quantitative measure is supplied by the quantum geometric tensor [66]

$$T_{ab\mathbf{k}} = \langle \partial_{k_a} u_{\mathbf{k}} | (1 - |u_{\mathbf{k}}\rangle\langle u_{\mathbf{k}}|) | \partial_{k_b} u_{\mathbf{k}} \rangle, \quad (1)$$

where $a, b = x, y, z$. The real part $g_{ab\mathbf{k}} = \text{Re}[T_{ab\mathbf{k}}]$, known as the quantum or Fubini-Study metric [36–38], captures the quantum distance under state variation $1 - |\langle u_{\mathbf{k}} | u_{\mathbf{k}+d\mathbf{k}} \rangle|^2 = g_{ab\mathbf{k}} dk_a dk_b$. On the other hand, the imaginary part measures the phase variation and the accompanying Berry flux $B_{a\mathbf{k}} = -\epsilon_{abc} \text{Im}[T_{bc\mathbf{k}}]$ [34, 67]. The nature of these quantities are elucidated transparently in an alternative expression. Define the Berry connection $\mathbf{A}_{\mathbf{k}} = \langle u_{\mathbf{k}} | i\nabla_{\mathbf{k}} | u_{\mathbf{k}} \rangle$ as a gauge field in momentum space, which is a manifestation of nontrivial band geometry [34].

The quantum metric and the Berry flux become

$$g_{ab\mathbf{k}} = \frac{1}{2} \langle u_{\mathbf{k}} | \{r_a, r_b\} | u_{\mathbf{k}} \rangle, \quad \mathbf{B}_{\mathbf{k}} = \nabla_{\mathbf{k}} \times \mathbf{A}_{\mathbf{k}}, \quad (2)$$

where the position $\mathbf{r} = i\nabla_{\mathbf{k}} - \mathbf{A}_{\mathbf{k}}$ serves as a momentum-space covariant derivative. The effect of Berry flux as a momentum-space “magnetic field” has been well-studied in the topological systems [34]. Here we focus on the quantum metric and search for useful indications to the nontrivial band geometry.

The individual components of quantum metric are usually complicated and hard to interpret. Nevertheless, the trace of quantum metric takes a profound form

$$\text{Tr}g_{\mathbf{k}} = \langle |\mathbf{r}|^2 \rangle, \quad (3)$$

where the expectation value $\langle \dots \rangle = \langle u_{\mathbf{k}} | \dots | u_{\mathbf{k}} \rangle$ of momentum-space Laplacian $|\mathbf{r}|^2$ is measured. Significantly, this quantity captures the “dual energy” of a free particle in momentum space, which carries a half-unity “dual mass” and experiences the Berry connection [35]. We thus establish a position-momentum duality between the band geometry and the free-particle motion under gauge field. This duality presents a feasible solution to the interpretation of the band geometry. If the duality leads to a simple free-electron model with well-studied solution, the trace of quantum metric can be understood under a direct inference.

We now introduce how the position-momentum duality operates in the topological systems. Here we focus on the 3D gapless topological systems, where approximate rotation symmetries can occur around the band crossings at low energy. With the approximate rotation symmetries, the duality to simple free-electron models becomes available. A band crossing can host a nontrivial defect of Berry connection, which induces nontrivial band geometry in the low-energy theory. We will show that such band geometry is encoded in a “dual energy quantization” in the trace of quantum metric. This scenario is eligible for both \mathbb{Z} and \mathbb{Z}_2 gapless topological systems.

We first conduct the duality-based analysis in the \mathbb{Z} gapless topological systems. As a paradigmatic example, we present the analysis of band geometry in the chiral multifold semimetals (CMS) [35]. The chiral multifold semimetals constitute a large family of \mathbb{Z} nodal-point semimetals, where the band crossings occur at distinct points [Fig. 1(a)] [2–5]. At each nodal point, the low-energy theory is characterized by the chiral fermions with multifold degeneracy [Fig. 2(a)]. A minimal model exhibits a spin- s Hamiltonian with integer or half-integer spin $s = 1/2, 1, 3/2, \dots$

$$\mathcal{H}_{\text{CMS},\mathbf{k}} = v\mathbf{k} \cdot \mathbf{S}. \quad (4)$$

Here v is the effective velocity, $\mathbf{k} = k\hat{\mathbf{k}}$ with magnitude k and direction $\hat{\mathbf{k}}$, and $\mathbf{S} = (S^x, S^y, S^z)$ is the spin- s representation. The model obeys a rotation symmetry around the nodal point $\mathbf{k} = \mathbf{0}$. There are $2s + 1$

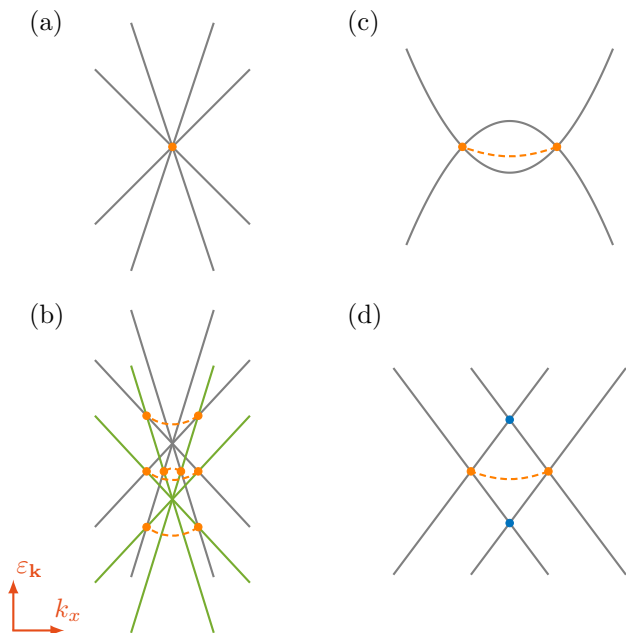


FIG. 2. The band structures in the minimal models for the (a) nodal-point, (b) nodal-surface, (c) \mathbb{Z}_2 -trivial nodal-loop, and (d) \mathbb{Z}_2 -nontrivial nodal-loop semimetals. The band crossings are indicated by the same colors as in Fig. 1. The points belonging to the same band crossing are connected by a dashed curve.

bands in this model, carrying the dispersion energies $\varepsilon_{\mathbf{k}}^{sn} = vkn$ with $n = -s, -s + 1, \dots, s$. In accordance with the Berry flux $\mathbf{B}_{\mathbf{k}}^{sn} = -(n/k^2)\hat{\mathbf{k}}$, the nodal point carries a quantized Berry monopole $q^{sn} = -n$. This monopole charge corresponds to the Chern number $C^{sn} = (1/2\pi) \oint d\mathbf{S}_{\mathbf{k}} \cdot \mathbf{B}_{\mathbf{k}}^{sn} = 2q^{sn} = -2n$ under an enclosing-surface integration, which is the topological invariant. The rotationally symmetric structure around the monopole indicates the duality to a Haldane sphere [63, 68, 69]. Analogous to the quantum Hall effect on the Haldane sphere, the “dual Landau level quantization” occurs in the trace of quantum metric in the chiral multifold semimetals [35]. An alternative form of the Hamiltonian $\tilde{\mathcal{H}}_{\text{CMS},\mathbf{k}} = ck\hat{\mathbf{k}} \cdot \mathbf{S}$ indicates that the wavefunctions are independent of k . Due to the absence of radial contribution, the trace of quantum metric $\text{Tr}g_{\text{CMS},\mathbf{k}}^{sn} = \langle |\mathbf{\Lambda}^{sn}|^2/k^2 \rangle$ measures the dual rotational energy of the dynamical angular momentum $\mathbf{\Lambda}^{sn} = \mathbf{r}^{sn} \times \mathbf{k}$. Note that the actual angular momentum under rotation symmetry takes the form $\mathbf{L}^{sn} = \mathbf{\Lambda}^{sn} + q^{sn}\hat{\mathbf{k}}$. With the relation $|\mathbf{\Lambda}^{sn}|^2 = |\mathbf{L}^{sn}|^2 - (q^{sn})^2$, we obtain the quantized trace of quantum metric

$$\text{Tr}g_{\text{CMS},\mathbf{k}}^{sn} = \frac{1}{k^2} [s(s+1) - (q^{sn})^2], \quad (5)$$

labeled by the angular momentum s and the monopole charge q^{sn} . This exemplifies the quantized band geometry from the dual Haldane sphere in the \mathbb{Z} nodal-point

semimetals.

The position-momentum duality can also be adopted to the \mathbb{Z} nodal-surface (NS) semimetals [20]. These systems accommodate two-band crossings in the form of closed surfaces [Fig. 1(b)]. The \mathbb{Z} nodal surface may be realized, for example, from a pair of degenerate chiral multifold semimetallic points. When the degeneracy is broken, an energy splitting $\Delta\varepsilon_0 = \varepsilon_0^+ - \varepsilon_0^- > 0$ occurs between the nodal points \mathbf{P}_{\pm} [Fig. 2(b)]. The bands from different nodal points cross at spherical surfaces, forming distinct nodal surfaces with two-band crossings. As the inflated nodal points [24], these nodal surfaces inherit the \mathbb{Z} topological structures of the original nodal points. Consider the low-energy theory of a nodal surface below charge neutrality, which is formed by the n_+ -th and n_- -th bands from the original nodal points. For the lower band of the nodal surface, the band eigenstate corresponds to the n_{\mp} -th original band inside(ouster) the nodal surface. This implies the occurrence of different Berry fluxes $\mathbf{B}_{\mathbf{k}}^{\text{in/out}} = \mathbf{B}_{\mathbf{k}}^{sn_{\mp}}$ and according Chern numbers $C^{\text{in/out}} = C^{sn_{\mp}}$ in the two regions. A topological invariant is defined by the change of Chern number across the nodal surface $\Delta C = C^{\text{in}} - C^{\text{out}}$ [20]. The quantum metric can also be inferred from the chiral multifold semimetals, with the individual components in the spin-1/2 case derived in Ref. 70. Here we explain the results in the framework of position-momentum duality. The low-energy theory is dual to a free-electron model with a “uniformly-charged magnetic spherical shell” and a magnetic monopole at the origin. While the monopole carries the charge $q = C^{\text{in}}/2$, the spherical shell carries the total charge $Q = \Delta C/2$ corresponding to the topological invariant. We thus obtain the trace of quantum metric under the dual Landau level quantization

$$\text{Tr}g_{\text{NS},\mathbf{k}}^{\text{in/out}} = \text{Tr}g_{\text{CMS},\mathbf{k}}^{sn_{\mp}}, \quad (6)$$

Analogous results are also obtained for the upper band of the nodal surface. Notably, the band geometry exhibit different structures on different sides of the nodal surface. This feature is attributed to the Berry charge at the nodal surface and is generic in the \mathbb{Z} nodal-surface semimetals.

We next turn to the analysis of \mathbb{Z}_2 gapless topological systems with the position-momentum duality. Before diving into the 3D systems, we discuss how the dual energy quantization occurs at the two-dimensional (2D) Dirac point (2DDP). This example will serve as an important hint to the 3D \mathbb{Z}_2 gapless topological systems. A minimal model at the 2D Dirac point takes a rotationally symmetric spin-1/2 form

$$\mathcal{H}_{2\text{DDP},\mathbf{k}} = v\mathbf{k} \cdot \boldsymbol{\sigma}, \quad (7)$$

where $\boldsymbol{\sigma} = (\sigma^x, \sigma^y)$ are the Pauli matrices. This system contains two bands with dispersion energies $\varepsilon_{\mathbf{k}}^{\pm} = \pm vk$, which become degenerate at the Dirac point $\mathbf{k} = \mathbf{0}$. The Berry connection forms a vortex structure around the

Dirac point, thereby driving a π phase winding in the band eigenstates. Accordingly, the Berry flux experiences a singularity at the Dirac point and vanishes everywhere else. The trace of quantum metric is determined based on this Berry vortex structure. According to the Hamiltonian $\mathcal{H}_{2\text{DDP},\mathbf{k}} = vk\mathbf{k}\cdot\boldsymbol{\sigma}$, the wavefunctions are k -independent. Without the radial contribution, the trace of quantum metric measures the dual rotational energy $\text{Tr}g_{2\text{DDP},\mathbf{k}}^n = \langle (\Lambda_z^n)^2/k^2 \rangle$ under rotation symmetry. Note that $\Lambda_z^n = L_z^n$ serves as the actual angular momentum since the Berry monopole is absent. The magnitude is set by the spin as $|L_z^n| = 1/2$, corresponding to the π phase winding around the Dirac point. We thus arrive at the trace of quantum metric

$$\text{Tr}g_{2\text{DDP},\mathbf{k}} = \frac{1}{4k^2}, \quad (8)$$

consistent with a direct calculation [50]. This indicates how the position-momentum duality works on the band geometry with Berry vortices.

The result at the 2D Dirac point can be generalized to the 3D \mathbb{Z}_2 gapless topological systems. A natural generalization occurs in the nodal-loop semimetals, where the band crossings take place along closed loops [Fig. 1(c)] [13–19]. Consider a minimal two-band model of the nodal-loop semimetals [23, 71]

$$\mathcal{H}_{\text{NL},\mathbf{k}} = \frac{k_\perp^2 - \Delta}{2m}\sigma^x + v_z k_z \sigma^y, \quad (9)$$

where $k_\perp = (k_x^2 + k_y^2)^{1/2}$ and $\Delta > 0$. This system shows a nodal loop in the k_x - k_y plane at charge neutrality [Fig. 2(c)], which is defined by the major radius $k_R = \sqrt{\Delta}$. A linearization at low energy leads to

$$\mathcal{H}_{\text{NL},\mathbf{k}} = v(k_\perp - k_R)\sigma^x + vk_z\sigma^y, \quad (10)$$

where isotropic dispersion around the nodal loop is assumed $v_\perp = k_R/m = v_z = v$. This linearized model obeys two rotation symmetries, which are about the nodal loop and the $k_\perp = 0$ line at loop center, respectively. The two bands in the linearized model exhibit the dispersion energies $\varepsilon_{\mathbf{k}}^\pm = \pm vk_r$. Here $k_r = [(k_\perp - k_R)^2 + k_z^2]^{1/2}$ is the minor radius from the nodal loop. Importantly, the nodal-loop system can be regarded as a “stacking” of the 2D Dirac-point systems along the nodal loop. This identifies the nodal loop as a Berry vortex line, which is a generalization from the Berry vortex at the 2D Dirac point. The π phase winding in the band eigenstates now occurs around the nodal loop. Accordingly, the Berry flux experiences a singularity along the nodal loop and vanishes everywhere else. The Berry vortex line induces the dual rotational energy of the axial angular momentum $|L_\phi^n| = 1/2$, where $\hat{\phi}$ is the tangent unit vector along the nodal loop. The trace of quantum metric is thus obtained as

$$\text{Tr}g_{\text{NL},\mathbf{k}} = \frac{1}{4k_r^2}, \quad (11)$$

similar to the result at the 2D Dirac point. Note that the nodal loop shrinks to a point and vanishes when Δ decreases and turns negative. Since the nodal loop can be annihilated by itself, it is called a \mathbb{Z}_2 -trivial nodal loop in the topological classification [15].

There also exist nodal loops which are \mathbb{Z}_2 -nontrivial [15, 17–19]. These nodal loops are realized in the systems with combined parity and time-reversal PT -symmetry, where the model and the band eigenstates are required to be real. Consider a minimal model of the \mathbb{Z}_2 -nontrivial nodal loops [15]

$$\mathcal{H}_{\mathbb{Z}_2\text{NL},\mathbf{k}} = vk_x\sigma^x + vk_y\tau^y\sigma^y + vk_z\sigma^z + m\tau^x\sigma^x, \quad (12)$$

where the Pauli matrices σ^a and τ^a are defined. This model accommodates four bands with the dispersion energies $\varepsilon_{\mathbf{k}}^{\pm\pm} = \pm v[(k_\perp \pm k_R)^2 + k_z^2]^{1/2}$ for $k_R = |m|/v$. At finite $|m| > 0$, the two middle bands form a nodal loop at charge neutrality with major radius k_R [Fig. 2(d)]. These two bands obey the same set of rotation symmetries as the system with \mathbb{Z}_2 -trivial nodal loop. Similar to the \mathbb{Z}_2 -trivial nodal loop, the nodal loop herein serves as a Berry vortex line for a π phase winding. An important difference is the interplay with an additional nodal line $k_\perp = 0$ at finite energy [19]. For the upper(lower) band, the additional nodal line occurs at the band crossing with the highest(lowest) band. This additional nodal line penetrates the center of the nodal loop, leading to a topologically nontrivial “link” [Fig. 1(d)]. The link with the nodal line defines a \mathbb{Z}_2 monopole at the nodal loop. This monopole drives the nodal loop \mathbb{Z}_2 -nontrivial, which shrinks to a point (when $m = 0$) at most under changing m . Note that the \mathbb{Z}_2 -nontrivial nodal loops can only be annihilated by a pair annihilation.

The link of the \mathbb{Z}_2 monopole is encoded in the band geometry. We calculate the quantum metric for the two middle bands in the minimal model. The individual components of quantum metric are complicated, with the special cases derived at $k_z = 0$ in Ref. 70. Despite the formal complexity, the wavefunctions are independent of the radial components k_r and k_R . This indicates the absence of radial contributions in the trace of quantum metric, leaving only the angular contributions

$$\text{Tr}g_{\mathbb{Z}_2\text{NL},\mathbf{k}} = \frac{1}{4k_r^2} + \frac{1}{4k_\perp^2}. \quad (13)$$

The first term is identical to the result of \mathbb{Z}_2 -trivial nodal loop, which is the dual rotational energy about the nodal loop. Meanwhile, the second term captures the dual rotational energy of the axial angular momentum $|L_z^n| = 1/2$ about the additional nodal line. The presence of this term clearly indicates the link of the \mathbb{Z}_2 monopole, which is absent for the \mathbb{Z}_2 -trivial nodal loop. We thus arrive at a clear interpretation of the nontrivial band geometry in the \mathbb{Z}_2 nodal-loop semimetals.

A direct manifestation of the band geometry occurs in the spread of Wannier functions [35, 40–42]. For

the Wannier functions of a band, the spread functional $\Omega = \langle \mathbf{r}^2 \rangle - \langle \mathbf{r} \rangle^2$ exhibits the gauge-invariant lower bound $\Omega_{\text{GI}} = \mathcal{V}_0 \Sigma$ with $\Sigma = \int_{\mathbf{k}} \text{Tr} g_{\mathbf{k}}$. Here \mathcal{V}_0 is the volume of a unit cell and $\int_{\mathbf{k}} = \int d^3 k / (2\pi)^3$. As the integrated trace of quantum metric, the gauge-invariant lower bound originates solely from the band geometry. A lower bound $\Sigma_{\text{SR}} = \int_{\text{SR}, \mathbf{k}} \text{Tr} g_{\mathbf{k}} \leq \Sigma$ can be further estimated by the focus on a subregion (SR). We consider this estimation in the 3D gapless topological systems, where the most significant contributions usually arise from the subregions near the band crossings. For the chiral multifold semimetals, the estimated lower bound $\Sigma_{\text{CMF}} = (\Lambda_k / 4\pi^2) G^{sn}$ is quantized [35]. Here $G^{sn} = (1/2\pi) \oint d\mathbf{S}_{\mathbf{k}} \cdot \hat{\mathbf{k}} \text{Tr} g_{\text{CMS}, \mathbf{k}}^{sn} = 2[s(s+1) - (q^{sn})^2]$ is a quantized enclosing-surface integration, and Λ_k is an ultraviolet (UV) cutoff of k . Note that the quantized result also applies to the \mathbb{Z} nodal-surface semimetals. The nodal-loop semimetals exhibit significantly different features. For the \mathbb{Z}_2 -trivial nodal loop, the estimated lower bound is logarithmically divergent $\Sigma_{\text{NL}} = (1/4\pi^2)(2\pi k_R)(1/4) \log k_r|_0^{\Lambda_{k_r}}$, where Λ_{k_r} defines the UV cutoff of k_r . This result is a direct generalization from the 2D Dirac point, where a logarithmic divergence also occurs. The \mathbb{Z}_2 -nontrivial nodal loop also exhibits this logarithmic divergence. Additionally, another logarithmic divergence $\sim \ln k_{\perp}|_0$ arises due to the link of the \mathbb{Z}_2 monopole. This distinguishes the estimated lower bound of the \mathbb{Z}_2 -nontrivial nodal loop from the \mathbb{Z}_2 -trivial one. Due to the logarithmic divergences, the band geometry may have stronger manifestations at the nodal loops than at the other band crossings.

The spread of Wannier functions manifests, for example, in the anomalous superfluid stiffness on flat bands [35, 49, 50, 53]. Such effect leads to the geometric enhancement of flat-band superconductivity, which are usually suppressed due to the low dispersion of electrons. The gauge-invariant lower bound can be probed directly with a periodic drive [39]. Consider a multiband system with the lowest band occupied. Under a linear shake along a direction $\hat{\mathbf{a}}$, the integrated quantum metric $\int_{\mathbf{k}} g_{aa\mathbf{k}}$ of the lowest band corresponds to the excitation rate. The integrated trace of quantum metric is then obtained from the measurements along all three directions $a = x, y, z$, which determines the gauge-invariant lower bound. Such a measurement has been performed experimentally in an ultracold atomic Floquet Chern insulator [44]. Most of the current measurements apply to the integrated trace of quantum metric in all occupied bands. The probe with momentum and band resolutions will advance the understanding of band geometry in the gapless topological systems. This may be achieved by, for example, the adiabatic-loading preparation of initial state in a particular band eigenstate [39, 72].

In summary, we show that the position-momentum duality offers a transparent interpretation of the band ge-

ometry at the topological band crossings. The trace of quantum metric provides a unified framework through this duality, which is achieved by encoding the dual rotational energy about the band crossings with nontrivial Berry defects. This scenario applies to the \mathbb{Z} nodal-point and nodal-surface semimetals, as well as the \mathbb{Z}_2 nodal-loop semimetals. While the symmetry-breaking perturbations, such as those far away from the band crossings, may break the simple quantization rules, the results may still remain close until the band crossing structures completely vanish. Our duality-based analysis offers a feasible route toward further understanding of the band geometry in the gapless topological systems. The investigations in the other gapless topological systems, such as the gapless topological superconductors [22–27], gapless spin liquids [28], degenerate bands with non-Abelian Berry connections, or higher-dimensional systems with tensor monopoles [64], may serve as interesting topics for future work.

The authors especially thank Rahul Nandkishore for fruitful discussions and feedback on the manuscript. YPL was sponsored by the Army Research Office under Grant No. W911NF-17-1-0482. The views and conclusions contained in this document are those of the authors and should not be interpreted as representing the official policies, either expressed or implied, of the Army Research Office or the U.S. Government. The U.S. Government is authorized to reproduce and distribute reprints for Government purposes notwithstanding any copyright notation herein. YPL also acknowledge Ying-Jer Kao for the hospitality at National Taiwan University during the pandemic.

-
- [1] C.-K. Chiu, J. C. Y. Teo, A. P. Schnyder, and S. Ryu, *Rev. Mod. Phys.* **88**, 035005 (2016).
 - [2] N. P. Armitage, E. J. Mele, and A. Vishwanath, *Rev. Mod. Phys.* **90**, 015001 (2018).
 - [3] B. Bradlyn, J. Cano, Z. Wang, M. G. Vergniory, C. Felser, R. J. Cava, and B. A. Bernevig, *Science* **353**, aaf5037 (2016).
 - [4] H. Isobe and L. Fu, *Phys. Rev. B* **93**, 241113 (2016).
 - [5] P. Tang, Q. Zhou, and S.-C. Zhang, *Phys. Rev. Lett.* **119**, 206402 (2017).
 - [6] I. Boettcher, *Phys. Rev. Lett.* **124**, 127602 (2020).
 - [7] Z. Rao, H. Li, T. Zhang, S. Tian, C. Li, B. Fu, C. Tang, L. Wang, Z. Li, W. Fan, J. Li, Y. Huang, Z. Liu, Y. Long, C. Fang, H. Weng, Y. Shi, H. Lei, Y. Sun, T. Qian, and H. Ding, *Nature* **567**, 496 (2019).
 - [8] D. S. Sanchez, I. Belopolski, T. A. Cochran, X. Xu, J.-X. Yin, G. Chang, W. Xie, K. Manna, V. Süß, C.-Y. Huang, N. Alidoust, D. Multer, S. S. Zhang, N. Shumiya, X. Wang, G.-Q. Wang, T.-R. Chang, C. Felser, S.-Y. Xu, S. Jia, H. Lin, and M. Z. Hasan, *Nature* **567**, 500 (2019).
 - [9] N. B. M. Schröter, D. Pei, M. G. Vergniory, Y. Sun, K. Manna, F. de Juan, J. A. Krieger, V. Süss, M. Schmidt, P. Dudin, B. Bradlyn, T. K. Kim,

- T. Schmitt, C. Cacho, C. Felser, V. N. Strocov, and Y. Chen, *Nat. Phys.* **15**, 759 (2019).
- [10] D. Takane, Z. Wang, S. Souma, K. Nakayama, T. Nakamura, H. Oinuma, Y. Nakata, H. Iwasawa, C. Cacho, T. Kim, K. Horiba, H. Kumigashira, T. Takahashi, Y. Ando, and T. Sato, *Phys. Rev. Lett.* **122**, 076402 (2019).
- [11] B. Q. Lv, Z.-L. Feng, J.-Z. Zhao, N. F. Q. Yuan, A. Zong, K. F. Luo, R. Yu, Y.-B. Huang, V. N. Strocov, A. Chikina, A. A. Soluyanov, N. Gedik, Y.-G. Shi, T. Qian, and H. Ding, *Phys. Rev. B* **99**, 241104 (2019).
- [12] N. B. M. Schröter, S. Stolz, K. Manna, F. de Juan, M. G. Vergniory, J. A. Krieger, D. Pei, T. Schmitt, P. Dudin, T. K. Kim, C. Cacho, B. Bradlyn, H. Bormann, M. Schmidt, R. Widmer, V. N. Strocov, and C. Felser, *Science* **369**, 179 (2020).
- [13] J.-M. Carter, V. V. Shankar, M. A. Zeb, and H.-Y. Kee, *Phys. Rev. B* **85**, 115105 (2012).
- [14] H. Weng, C. Fang, Z. Fang, B. A. Bernevig, and X. Dai, *Phys. Rev. X* **5**, 011029 (2015).
- [15] C. Fang, Y. Chen, H.-Y. Kee, and L. Fu, *Phys. Rev. B* **92**, 081201 (2015).
- [16] Q.-F. Liang, J. Zhou, R. Yu, Z. Wang, and H. Weng, *Phys. Rev. B* **93**, 085427 (2016).
- [17] Y. X. Zhao and Y. Lu, *Phys. Rev. Lett.* **118**, 056401 (2017).
- [18] T. Bzdušek and M. Sigrist, *Phys. Rev. B* **96**, 155105 (2017).
- [19] J. Ahn, D. Kim, Y. Kim, and B.-J. Yang, *Phys. Rev. Lett.* **121**, 106403 (2018).
- [20] O. Türker and S. Moroz, *Phys. Rev. B* **97**, 075120 (2018).
- [21] W. Wu, Y. Liu, S. Li, C. Zhong, Z.-M. Yu, X.-L. Sheng, Y. X. Zhao, and S. A. Yang, *Phys. Rev. B* **97**, 115125 (2018).
- [22] M. Sigrist and K. Ueda, *Rev. Mod. Phys.* **63**, 239 (1991).
- [23] R. Nandkishore, *Phys. Rev. B* **93**, 020506 (2016).
- [24] D. F. Agterberg, P. M. R. Brydon, and C. Timm, *Phys. Rev. Lett.* **118**, 127001 (2017).
- [25] P. M. R. Brydon, D. F. Agterberg, H. Menke, and C. Timm, *Phys. Rev. B* **98**, 224509 (2018).
- [26] J. W. F. Venderbos, L. Savary, J. Ruhman, P. A. Lee, and L. Fu, *Phys. Rev. X* **8**, 011029 (2018).
- [27] J. M. Link and I. F. Herbut, *Phys. Rev. Lett.* **125**, 237004 (2020).
- [28] L. Savary and L. Balents, *Rep. Prog. Phys.* **80**, 016502 (2016).
- [29] N. R. Cooper, J. Dalibard, and I. B. Spielman, *Rev. Mod. Phys.* **91**, 015005 (2019).
- [30] B. Song, C. He, S. Niu, L. Zhang, Z. Ren, X.-J. Liu, and G.-B. Jo, *Nat. Phys.* **15**, 911 (2019).
- [31] T. Ozawa, H. M. Price, A. Amo, N. Goldman, M. Hafezi, L. Lu, M. C. Rechtsman, D. Schuster, J. Simon, O. Zeitlinger, and I. Carusotto, *Rev. Mod. Phys.* **91**, 015006 (2019).
- [32] X. Tan, D.-W. Zhang, Q. Liu, G. Xue, H.-F. Yu, Y.-Q. Zhu, H. Yan, S.-L. Zhu, and Y. Yu, *Phys. Rev. Lett.* **120**, 130503 (2018).
- [33] X. Tan, Y. X. Zhao, Q. Liu, G. Xue, H.-F. Yu, Z. D. Wang, and Y. Yu, *Phys. Rev. Lett.* **122**, 010501 (2019).
- [34] D. Xiao, M.-C. Chang, and Q. Niu, *Rev. Mod. Phys.* **82**, 1959 (2010).
- [35] Y.-P. Lin and W.-H. Hsiao, *Phys. Rev. B* **103**, L081103 (2021).
- [36] J. P. Provost and G. Vallee, *Commun. Math. Phys.* **76**, 289 (1980).
- [37] D. N. Page, *Phys. Rev. A* **36**, 3479 (1987).
- [38] J. Anandan and Y. Aharonov, *Phys. Rev. Lett.* **65**, 1697 (1990).
- [39] T. Ozawa and N. Goldman, *Phys. Rev. B* **97**, 201117 (2018).
- [40] N. Marzari and D. Vanderbilt, *Phys. Rev. B* **56**, 12847 (1997).
- [41] S. Matsuura and S. Ryu, *Phys. Rev. B* **82**, 245113 (2010).
- [42] N. Marzari, A. A. Mostofi, J. R. Yates, I. Souza, and D. Vanderbilt, *Rev. Mod. Phys.* **84**, 1419 (2012).
- [43] O. Bleu, D. D. Solnyshkov, and G. Malpuech, *Phys. Rev. B* **97**, 195422 (2018).
- [44] L. Asteria, D. T. Tran, T. Ozawa, M. Tarnowski, B. S. Rem, N. Fläschner, K. Sengstock, N. Goldman, and C. Weitenberg, *Nat. Phys.* **15**, 449 (2019).
- [45] R. L. Klees, G. Rastelli, J. C. Cuevas, and W. Belzig, *Phys. Rev. Lett.* **124**, 197002 (2020).
- [46] M. Yu, P. Yang, M. Gong, Q. Cao, Q. Lu, H. Liu, S. Zhang, M. B. Plenio, F. Jelezko, T. Ozawa, N. Goldman, and J. Cai, *Nat. Sci. Rev.* **7**, 254 (2019).
- [47] X. Tan, D.-W. Zhang, Z. Yang, J. Chu, Y.-Q. Zhu, D. Li, X. Yang, S. Song, Z. Han, Z. Li, Y. Dong, H.-F. Yu, H. Yan, S.-L. Zhu, and Y. Yu, *Phys. Rev. Lett.* **122**, 210401 (2019).
- [48] A. Gianfrate, O. Bleu, L. Dominici, V. Ardizzone, M. De Giorgi, D. Ballarini, G. Lerario, K. W. West, L. N. Pfeiffer, D. D. Solnyshkov, D. Sanvitto, and G. Malpuech, *Nature* **578**, 381 (2020).
- [49] S. Peotta and P. Törmä, *Nat. Commun.* **6**, 8944 (2015).
- [50] L. Liang, T. I. Vanhala, S. Peotta, T. Siro, A. Harju, and P. Törmä, *Phys. Rev. B* **95**, 024515 (2017).
- [51] X. Hu, T. Hyart, D. I. Pikulin, and E. Rossi, *Phys. Rev. Lett.* **123**, 237002 (2019).
- [52] F. Xie, Z. Song, B. Lian, and B. A. Bernevig, *Phys. Rev. Lett.* **124**, 167002 (2020).
- [53] Y.-P. Lin, *Phys. Rev. Research* **2**, 043209 (2020).
- [54] T. Neupert, C. Chamon, and C. Mudry, *Phys. Rev. B* **87**, 245103 (2013).
- [55] P. Zanardi, P. Giorda, and M. Cozzini, *Phys. Rev. Lett.* **99**, 100603 (2007).
- [56] Y.-Q. Ma, S. Chen, H. Fan, and W.-M. Liu, *Phys. Rev. B* **81**, 245129 (2010).
- [57] M. Kolodrubetz, V. Gritsev, and A. Polkovnikov, *Phys. Rev. B* **88**, 064304 (2013).
- [58] R. Roy, *Phys. Rev. B* **90**, 165139 (2014).
- [59] M. Claassen, C. H. Lee, R. Thomale, X.-L. Qi, and T. P. Devereaux, *Phys. Rev. Lett.* **114**, 236802 (2015).
- [60] A. Srivastava and A. Imamoğlu, *Phys. Rev. Lett.* **115**, 166802 (2015).
- [61] Y. Gao, S. A. Yang, and Q. Niu, *Phys. Rev. B* **91**, 214405 (2015).
- [62] F. Piéchon, A. Raoux, J.-N. Fuchs, and G. Montambaux, *Phys. Rev. B* **94**, 134423 (2016).
- [63] F. D. M. Haldane, *Phys. Rev. Lett.* **51**, 605 (1983).
- [64] G. Palumbo and N. Goldman, *Phys. Rev. Lett.* **121**, 170401 (2018).
- [65] Y. Hwang, J. Jung, J.-W. Rhim, and B.-J. Yang, arXiv e-prints, arXiv:2012.15122 (2020), arXiv:2012.15122 [cond-mat.mes-hall].
- [66] M. V. Berry, in *Geometric Phases in Physics*, edited by A. Shapere and F. Wilczek (World Scientific, Singapore, 1989) p. 7.
- [67] M. V. Berry, *Proc. R. Soc. London, Ser. A* **392**, 45 (1984).

- [68] J. K. Jain, *Composite Fermions* (Cambridge University Press, Cambridge, 2007).
- [69] W.-H. Hsiao, [Phys. Rev. B **101**, 155310 \(2020\)](#).
- [70] G. Salerno, N. Goldman, and G. Palumbo, [Phys. Rev. Research **2**, 013224 \(2020\)](#).
- [71] Y. Huh, E.-G. Moon, and Y. B. Kim, [Phys. Rev. B **93**, 035138 \(2016\)](#).
- [72] M. Aidelsburger, M. Lohse, C. Schweizer, M. Atala, J. T. Barreiro, S. Nascimbène, N. R. Cooper, I. Bloch, and N. Goldman, [Nat. Phys. **11**, 162 \(2015\)](#).